



Reconnection Acceleration in Saturn's Dayside Magnetodisk: A Multicase Study with *Cassini*

R. L. Guo^{1,2} , Z. H. Yao² , N. Sergis^{3,4} , Y. Wei^{1,5}, D. Mitchell⁶, E. Roussos⁷, B. Palmaerts² ,
W. R. Dunn⁸ , A. Radioti², L. C. Ray⁹ , A. J. Coates⁸ , D. Grodent² , C. S. Arridge⁹,
P. Kollmann⁶ , N. Krupp⁷, J. H. Waite¹⁰ , M. K. Dougherty¹¹ , J. L. Burch¹⁰, and W. X. Wan^{1,5}

¹ Key Laboratory of Earth and Planetary Physics, Institute of Geology and Geophysics, Chinese Academy of Sciences, Beijing, People's Republic of China

² Laboratoire de Physique Atmospherique et Planetaire, STAR institute, Universite de Liege, Liege, Belgium

³ Office for Space Research and Technology, Academy of Athens, Athens, Greece

⁴ Institute of Astronomy, Astrophysics, Space Applications and Remote Sensing, National Observatory of Athens, Athens, Greece

⁵ College of Earth and Planetary Sciences, University of Chinese Academy of Sciences, Beijing, People's Republic of China

⁶ Applied Physics Laboratory, Johns Hopkins University, Laurel, Maryland, USA

⁷ Max-Planck-Institute für Sonnensystemforschung, Göttingen, Germany

⁸ Mullard Space Science Laboratory, University College London, Holmbury St Mary, Dorking RH5 6NT, UK

⁹ Department of Physics, Lancaster University, Bailrigg, Lancaster LA1 4 YB, UK

¹⁰ Southwest Research Institute, San Antonio, TX, USA

¹¹ Faculty of Natural Sciences, Department of Physics, Imperial College, London, UK

Received 2018 October 9; revised 2018 October 29; accepted 2018 October 31; published 2018 November 20

Abstract

Recently, rotationally driven magnetic reconnection was first discovered in Saturn's dayside magnetosphere. This newly confirmed process could potentially drive bursty phenomena at Saturn, i.e., pulsating energetic particles and auroral emissions. Using *Cassini*'s measurements of magnetic fields and charged particles, we investigate particle acceleration features during three magnetic reconnection events observed in Saturn's dayside magnetodisk. The results suggest that the rotationally driven reconnection process plays a key role in producing energetic electrons (up to 100 keV) and ions (several hundreds of kiloelectron volts). In particular, we find that energetic oxygen ions are locally accelerated at all three reconnection sites. Isolated, multiple reconnection sites were recorded in succession during an interval lasting for much less than one Saturn rotation period. Moreover, a secondary magnetic island is reported for the first time at the dayside, collectively suggesting that the reconnection process is not steady and could be "drizzle-like." This study demonstrates the fundamental importance of internally driven magnetic reconnection in accelerating particles in Saturn's dayside magnetosphere, and likewise in the rapidly rotating Jovian magnetosphere and beyond.

Key words: acceleration of particles – magnetic reconnection – planetary systems

1. Introduction

Magnetic reconnection is a fundamental physical process that converts energy and accelerates charged particles in cosmic, laboratory, and space plasma environments (Zweibel & Yamada 2009). Magnetic reconnection changes the magnetic topology of a system and can couple different plasma populations (Hesse et al. 2017). This process plays a pivotal role in driving the interaction between external interplanetary magnetic fields and internal planetary magnetic fields (Dungey 1961), as well as driving the plasma dynamics inside planetary magnetospheres (e.g., in the nightside planetary magnetotails Hones 1979; Arridge et al. 2016).

Direct evidence of magnetopause reconnection has been reported at Earth (Paschmann et al. 1979) and other planets such as Mercury (Slavin et al. 2009) and Saturn (McAndrews et al. 2008). In the nightside magnetotail of Earth and Mercury, magnetic reconnection is considered to release the nightside magnetic energy that is accumulated via dayside magnetopause reconnection and plasma circulation. Magnetic reconnection and its consequent production of plasmoids and secondary islands also play important roles on magnetic flux closure in the

nightside of Saturn's magnetosphere (Jackman et al. 2011; Arridge et al. 2016).

The Kronian and Jovian magnetospheres are, however, significantly different from the terrestrial and hermean magnetospheres for two major reasons: (1) their magnetospheres rotate much more rapidly, (2) they have internal plasma sources from their rings and moons, which inject hot plasmas into the magnetosphere system. Internally produced plasma in rapidly rotating magnetic environments is radially transported outward (Bagenal et al. 2016), and causes the magnetosphere to attain a stretched magnetic field configuration, termed the magnetodisk. Similar to the terrestrial and hermean magnetospheres, magnetic reconnection at Jupiter and Saturn has also been identified at their magnetopauses and the magnetotails (Huddleston et al. 1997; Badman et al. 2013; Arridge et al. 2016; Masters 2017). Moreover, the magnetic reconnection process on the nightside of the giant planetary magnetospheres can be driven not only by solar wind energy, but also by internal energy, known as internally driven magnetic reconnection (Vasyliunas 1983; Kronberg et al. 2007; Jackman et al. 2011). By surveying magnetic measurements from the *Cassini*-MAG instrument, Delamere et al. (2015) revealed that the reconnection indicator (i.e., negative signature of the B_θ magnetic component in Kronographic Radial-Theta-Phi (KRTP) coordinates, a spherical polar coordinates) could exist at all local times, including high probabilities of occurrence at



Original content from this work may be used under the terms of the [Creative Commons Attribution 3.0 licence](https://creativecommons.org/licenses/by/3.0/). Any further distribution of this work must maintain attribution to the author(s) and the title of the work, journal citation and DOI.

the unexpected pre-noon sectors, and suggested that the reconnection processes were “drizzle-like” that occur at small patchy regions. Plasma injection into Saturn’s inner magnetosphere is also revealed to exist at all local times (Azari et al. 2018). Guo et al. (2018) directly confirmed the existence of magnetic reconnection in Saturn’s dayside magnetodisk (i.e., well inside the magnetopause) by examining the reconnection-associated Hall current system and the reconnection acceleration plasma features (including electrons and ions). They showed that heavy ions were accelerated up to 600 keV by the dayside magnetodisk reconnection (DMR). Following the DMR signature, 1 hr pulsating energetic electrons were observed, while it is unclear whether the coexistence of DMR and pulsating energetic electrons is a coincidence or if the two processes are physically connected. The quasi-periodic energetic electron pulsation signatures have been reported in many studies at many local times (Mitchell et al. 2009; Palmaerts et al. 2016b; Roussos et al. 2016; Yates et al. 2016), and have been suggested to be relevant to the pulsating auroral emissions (Badman et al. 2015; Palmaerts et al. 2016a).

In this study, we identify three DMR events and investigate the associated energetic particle features by using *Cassini*’s multi-instrument measurements. We report details of energetic oxygen ions and electrons in the reconnection region. Pitch angle features of hot electrons are also analyzed for each reconnection process.

2. *Cassini* Observations of Reconnection Events

We analyze magnetic field observations from the *Cassini*-MAG instrument (Dougherty et al. 2004), thermal ion and electron measurements with energy range up to 28 keV (electrons) and 50 keV (ions) from *Cassini*-CAPS/IMS/ELS (Young et al. 2004), and energetic (>18 keV (electrons) and >27 keV (ions)) particle data from the Low-Energy Magnetospheric Measurements System (LEMMS) and the Ion and Neutral Camera (INCA) of the Magnetosphere Imaging Instrument (MIMI) (Krimigis et al. 2004). Hot electron pitch angle information is available by combining the in-situ magnetic field and particle data.

Reconnection diffusion region is the key region of the magnetic reconnection domain. However, this region is very small and dynamic, and it is very difficult to explore this with a spacecraft. From a realistic perspective, the negative B_θ signature is usually adopted as a simplified indicator of the magnetic reconnection, which can also effectually expose the reconnection diffusion region. We surveyed the *Cassini* data that were collected from 2005 to 2012, and obtained 139 events that contain negative B_θ signatures inside the magnetosphere at the noon sector from 9 LT (Local Time) to 15 LT, with latitude inside 30° . There are 33 events showing correlations between the negative B_θ signatures and the flux increases of the energetic oxygen ion, which is one of the most important species at Saturn. In this work, we identify three reconnection diffusion events from the 33 events, and investigate their Hall magnetic signatures and their ambient plasma features.

3. Event 1: 2005 November 25

Figure 1(a) shows magnetic field components in KRTP coordinates for 2005 November 25 between 11:40 UT and 13:40 UT. Figure 1(b) shows the magnetic field components in the X-line coordinate system (Arridge et al. 2016), which is a

rectangular coordinate system that removes the bend-back effect of the magnetic field lines in the magnetodisk. Figure 1(c) shows energetic electron differential flux from 18 to 832 keV measured by the MIMI-LEMMS instrument. Figure 1(d) shows the energy spectrogram of omnidirectional hot electron flux measured by the CAPS-ELS instrument, and Figures 1(e)–(g) show pitch angle distribution for electrons within three different energy ranges, i.e., from 50 eV to 500 eV, 500 eV to 3 keV, and 3 keV to 28 keV. As shown in Figures 1(e)–(g), the coverage of pitch angles during the whole period was poor, which is a common situation in *Cassini*’s CAPS-ELS data set, due to the limited field of view of the instrument. Figure 1(h) shows energetic ion (generally protons) differential flux from 27 keV to 4 MeV from the MIMI-LEMMS instrument. Figure 1(i) shows the energy spectrogram for omnidirectional ion flux from the CAPS-IMS instrument. Figure 1(j) shows the energetic oxygen differential flux from 46 keV to nearly 1 MeV from the MIMI-INCA instrument.

Following the negative B_θ signature in Figure 1(a) (or positive B_Z component in Figure 1(b)) at $\sim 12:13$ UT and $\sim 13:10$ UT, two magnetic reconnection sites (highlighted in pink) were detected by *Cassini* in the pre-noon sector (at 9 LT) at a radial distance of $\sim 21 R_S$ (Saturn’s Radius, $1R_S = 60,268$ km) from Saturn’s center. Moreover, B_Y changes sign when B_Z reverses, which is consistent with reconnection-produced Hall magnetic fields (Arridge et al. 2016; Guo et al. 2018). As suggested by the correspondingly small $|B_r|$, the spacecraft was in the outflow part of the reconnection region when the negative B_θ was detected.

The electron spectrograms (Figure 1(d)) in the reconnection regions are featured by higher than the ambient plasma energies. The background region (before the highlighted intervals) where electrons have a wide energy region from 10 s of eV to ~ 1 keV, while electrons in the reconnection sites are mostly from 100 s to a few keV. The pitch angle distributions in Figures 1(e)–(g) showed that the electrons in these reconnection sites are approximately isotropic, but are field-aligned outside the reconnection regions. The isotropic pitch angle distribution of electrons is a typical feature of the magnetic reconnection outflow region (e.g., Wang et al. 2016).

The energetic electron flux (in Figure 1(c)) is enhanced during the two negative B_θ intervals and is also correlated to the magnitude of the B_r component. When $|B_r| > 3$ nT, the electron flux in both Figures 1(c) and (d) minimizes, suggesting that the spacecraft was away from the current sheet center. Before the second highlighted region, the energetic electron flux is also increased when $|B_r|$ decreases, suggesting that the reconnection processes have been proceeding for a while and the accelerated electrons have filled in the current sheet. In addition, as shown in Figure 1(d), the central energy of the electron flux in the second reconnection site is higher than that in the first one. Moreover, the fluxes of energetic protons (tens of keV to >100 keV, shown in Figure 1(h)) and energetic oxygen ions (>200 keV, shown in Figure 1(j)) are mainly enhanced in the second reconnection site. The enhancement of thermal ions (<10 keV) in the first reconnection site can be clearly seen in the ion spectrogram in Figure 1(i). The two reconnection events detected nearby have significantly different accelerating features, which might suggest that they are two individual reconnection sites, and therefore it is consistent with the “drizzle-like” reconnection picture.

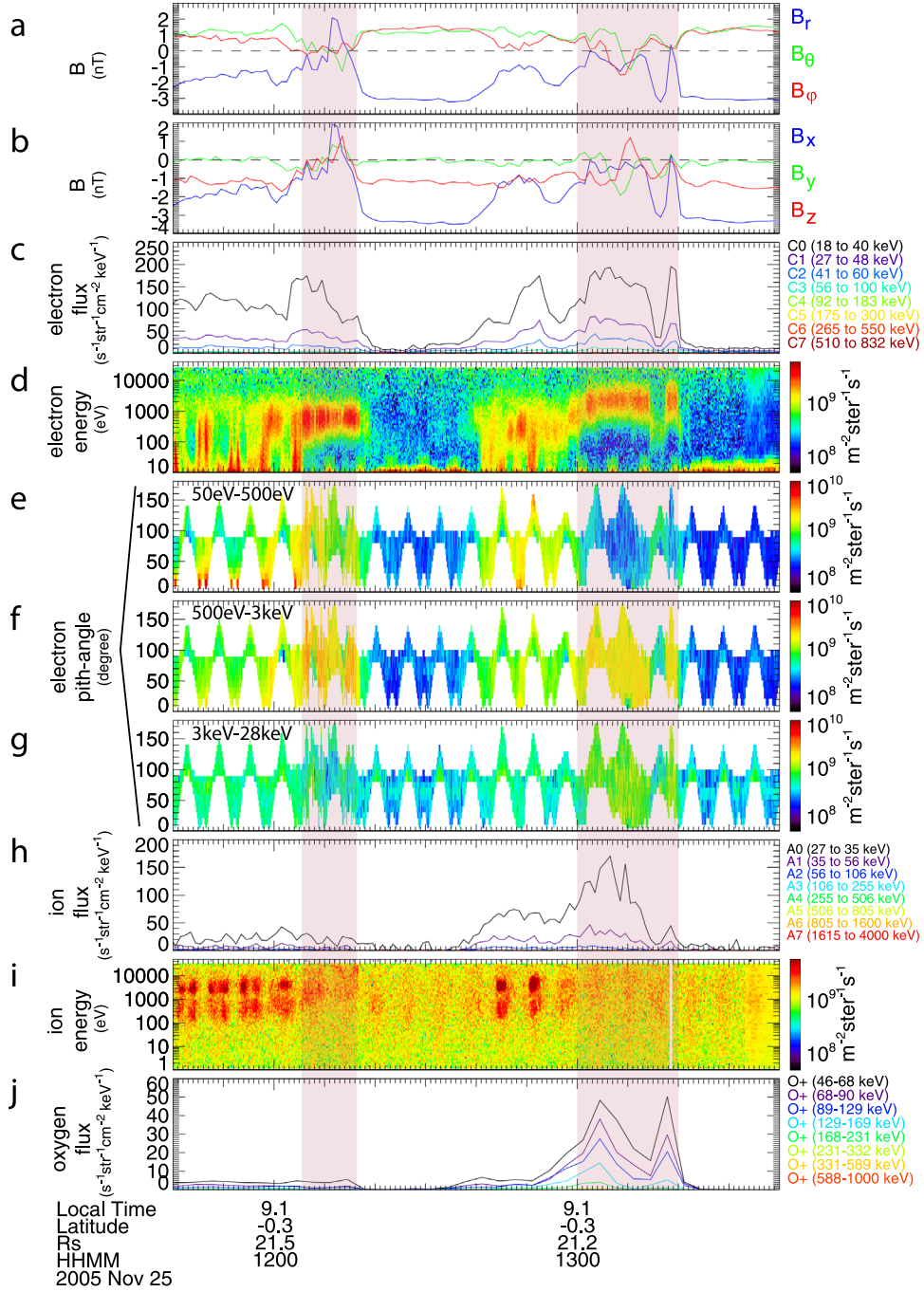


Figure 1. Dayside magnetodisk reconnection event on 2005 November 25. (a) Three magnetic field components in KRTP coordinates (B_r in blue, B_θ in green and B_ϕ in red), and (b) in reconnection coordinates (B_x in blue, B_y in green and B_z in red). (c) Energetic electron differential flux from MIMI-LEMMS. (d) Energy spectrogram of omnidirectional electron flux from CAPS-ELS. (e)–(g) Pitch angle distribution for electrons within energy ranges of 50 eV to 500 eV, 500 eV to 3 keV, and 3 keV to 28 keV. (h) Energetic proton differential flux from MIMI-LEMMS. (i) Energy spectrogram for omnidirectional ion flux from CAPS-IMS. (j) Energetic oxygen differential flux from MIMI-INCA. The pink regions highlighted the two reconnection regions that are identified by combining the signatures of the negative B_θ component, the Hall magnetic field, and the heated electrons.

4. Event 2: 2008 September 15

Figure 2 shows the second event that occurred on 2008 September 15 between 11:00 UT and 16:00 UT, in the near-noon sector (at 11.2 LT) and at a radial distance of $\sim 18 R_s$. The large magnitude of the B_r component was expected since *Cassini* was at high latitudes, similar to the case in Guo et al. (2018), implying that the spacecraft was in the outer layer of the current sheet. The negative B_θ signature in Figure 2(a)

lasted for more than 2 hr from $\sim 11:43$ UT to $\sim 14:24$ UT and is followed by a bipolar B_θ signature around 14:53 UT.

The distinct structure at around 14:53 UT is likely a secondary island (highlighted in pink) inside the long-lasting negative B_θ interval. Additionally, in the X-line coordinates (Figure 2(b)), the bipolar signature of the B_y component is consistent with the Hall magnetic fields. The perpendicular flux of hot electrons is enhanced in the positive B_θ region of the secondary island (Figures 2(e) and (f)), while it is field-aligned

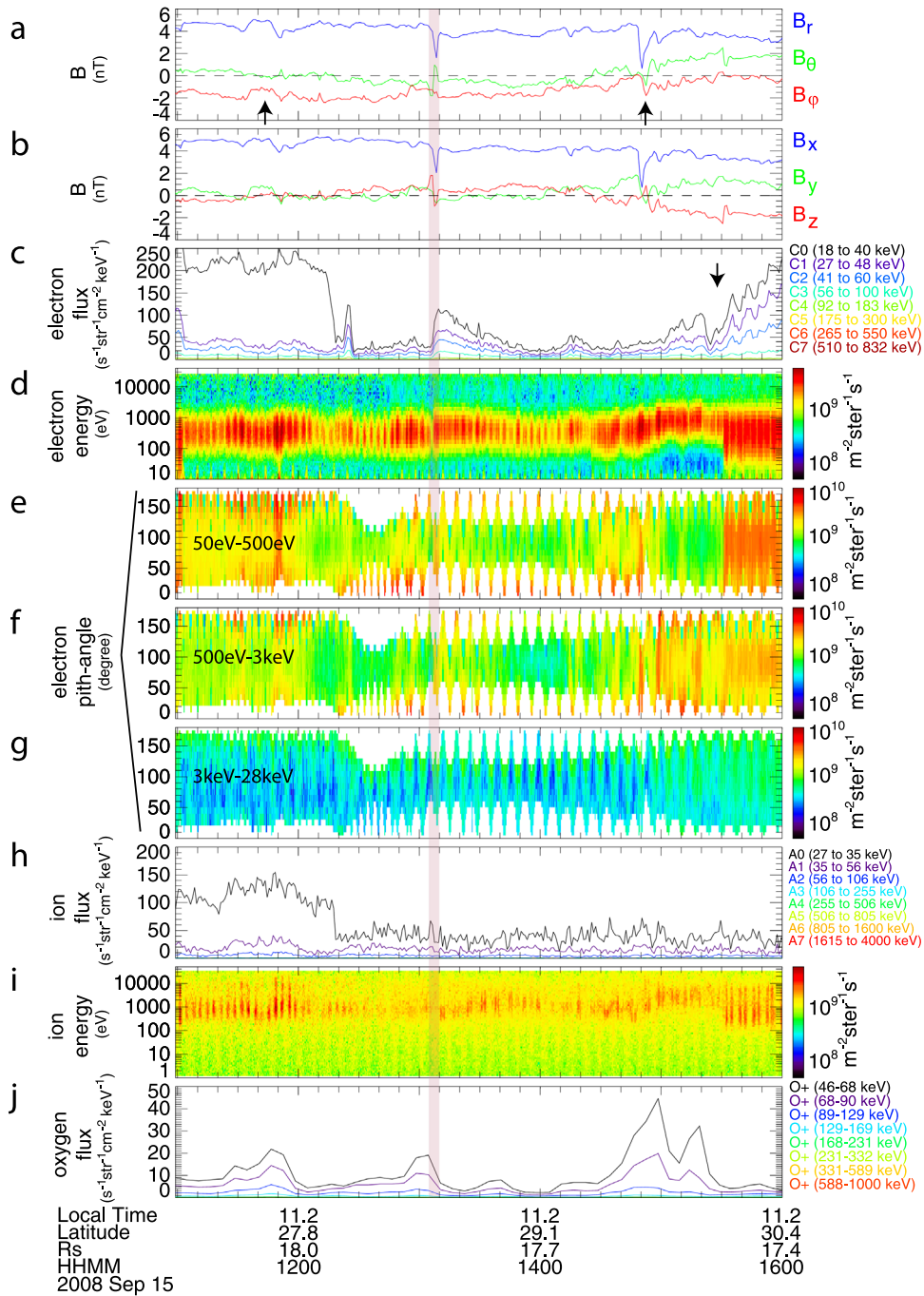


Figure 2. Dayside magnetodisk reconnection event on 2008 September 15. The panels are arranged in the same format as Figure 1. The high electron/ion fluxes from C0/A0 channel at the beginning of Figures 2(c)/(h) are due to light contamination.

in the rest of the long-lasting negative B_θ region. There is no signature in Figure 2(d) to show that electrons are substantially accelerated inside the secondary island, suggesting that this secondary island is not contracting. This is because that contracting secondary island would strongly energize electrons (Drake et al. 2006). The energetic oxygen flux (Figure 2(j)) enhances ahead of the encounter with the secondary island, while the energetic electron flux (Figure 2(c)) increases after the encounter with the positive B_θ region of the secondary island and keeps a high level outside the secondary island, which might have originated from other nearby secondary reconnection sites that generated the secondary island. Besides the secondary island region, the energetic oxygen flux also

enhances at the onset of the long-lasting negative B_θ region (marked by the first arrow in Figure 2(a)) and at the end of the negative B_θ region (marked by the second arrow in Figure 2(a)). After $\sim 15:30$ UT, while the energetic electron flux increases sharply (marked by the black arrow in Figure 2(c)), the electron spectrogram in Figure 2(d) broadens to contain electrons with energy less than 100 eV. The pitch angle for the broadband electron spectrogram is largely enhanced at perpendicular (Figures 2(e) and (f)), opposite to the bidirectional feature during the negative B_θ interval. The pitch angle distributions of this event are different from those of the first event where the electrons showed many isotropic features in the negative B_θ region while bidirectional in the

background. In the event of Figure 2, bidirectional electrons are also seen in the negative B_θ region. The difference between the two events might be due to the relative positions between *Cassini* and the current sheet, as the spacecraft’s latitude in the second event was much higher than that in the first event. Hence, *Cassini* may be detecting the outer edge of the current sheet, which could have different plasma characteristics compared to the current center. It could also be due to aperiodic short timescale dynamics that often dominate locally.

5. Event 3: 2008 April 15

The third reconnection event was also observed in the near-noon sector (at 11.5 LT) with a radial distance of $\sim 23 R_S$. Figure 3 is organized in the same manner as Figures 1 and 2, and shows data from 2008 April 14 21:40 UT to 2008 April 15 01:40 UT. There is a short negative B_θ region (transient 1) around 14 April 2008 23:15 UT (dashed vertical line). After transient 1, the B_θ component shows a significant bipolar signature (transient 2) with oscillations between 14 April 23:47 UT to 15 April 00:33 UT (highlighted in pink).

In transient 2, the corresponding Hall magnetic field is obvious in Figure 3(b) where the B_Y component reverses from positive to negative. In Figure 3(f), the electrons with energies from 500 eV to 3 keV in this interval are enhanced both in the perpendicular and antiparallel directions (we lack parallel information due to the instrument’s limited field of view), suggesting that this could be the electron exhaust region, which is the inner part of the reconnection region and is filled by energized electrons that have been accelerated by both the X-line and a parallel potential near the separatrix region (e.g., Egedal et al. 2012 and Wang et al. 2016).

The energetic electron flux in Figure 3(c) is enhanced when B_θ attained large positive values during transient 2. The energetic oxygen flux increases on both sides of the B_θ bipolar interval and drops at the same time that the energetic electrons are suddenly enhanced. Considering that the electron diffusion region is much smaller than and is surrounded by the oxygen diffusion region, the features of energized plasma can suggest that the spacecraft moved from the oxygen diffusion region on the outer part of the reconnection region (the first oxygen flux enhancement during the transient 2), to the electron exhaust further inside the reconnection region (the oxygen flux decreases and meanwhile electron flux enhances during the transient 2), and then back to the oxygen diffusion region (the second oxygen flux enhancement during the transient 2).

In transient 1, the B_ϕ component was nearly zero before B_θ became negative, suggesting the azimuthal bend-back configuration of the magnetodisk (Vasyliunas 1983) is mostly eliminated by the reconnection process in this region. Revealed by the plasma properties, the reconnection signatures observed at transient 1 can be divided into three regions, which are indicated above Figure 3(d) with three horizontal arrows.

The first region is where the energetic oxygen and proton fluxes were enhanced, in Figures 3(j) and (h), respectively. The electron spectrogram (Figure 3(d)) shows a cavity in the low-energy range. Electrons with energy around 1 keV display a bidirectional pitch angle distribution (Figure 3(f)), but they are more isotropic above 3 keV (Figure 3(g)). The second region is after the cold electron cavity and before the peak of the B_θ component. The energetic electron flux in Figure 3(c) was sharply enhanced in this region. The electron spectrogram has two bands. The low-energy band is associated with

bidirectional features (Figure 3(e)), and the high-energy band is roughly isotropic (Figure 3(f)). The third region is where the B_θ component sharply drops to negative. The electron spectrogram here is again bimodal. The flux of the low-energy electron band is enhanced in the perpendicular direction (Figure 3(e)).

The double electron bands in transient 1 are likely the mixture of reconnection accelerated population and ambient population. Enhancements in the low-energy electron band are correlated with the dips in B_r . The four groups of colored arrows above Figures 3(a) and (d) show the correspondence between the B_r dips and intensifications in the low-energy electron bands. This correlation strongly indicates that the low-energy electron population could only exist in the inner current sheet, while the high-energy electron population could reach distances farther from the current sheet center (Sergis et al. 2011). The electron population in this event appeared to have different characteristics compared to the other two events presented in this work. A further statistical study of the electron properties at different radial distances, local times, and latitudes is required to systematically understand the variable behavior of electrons in different events.

6. Discussion and Conclusion

As suggested by Delamere et al. (2015), magnetic reconnection can be expected to occur at any local time and not only in the midnight sector. The unambiguous ion diffusion region reported by Guo et al. (2018) and the three reconnection cases in this study, provide additional and direct evidence of the existence of the DMR processes, which locally produce energetic electrons and ions with energies of 100 s of keV at the dayside magnetosphere.

Figure 4 shows the line plots and the energy spectrograms for the flux of energetic hydrogen (top two panels) and oxygen (bottom two panels) during the enhancement in the first event studied here (the second highlighted region in Figure 1). The flux peaks across all the energies of the hydrogen and oxygen ions at the same time, eliminating the possibility that our signatures were generated by an injection event and suggesting that the ions were locally accelerated. The spectrogram is similar to that reported in Angelopoulos et al. (2008) for a terrestrial magnetotail reconnection event. It is readily expected that the flux would enhance (drop) when moving toward (away from) the reconnection region, since the magnetic reconnection domain is the source region of energetic particles.

Observational features from the three events support the concept of the “drizzle-like” reconnection process, i.e., reconnection on global scales facilitated through numerous, small-scale reconnection channels (Delamere et al. 2015). For the event on 2005 November 25 (Figure 1), the energy of the hot electrons in the second reconnection site is higher than the first one (Figure 1(d)). Furthermore, the >10 keV energetic ions prominently appear in the second reconnection site, while it was much quieter in the first one (Figures 1(h) and (j)). These differences between the accelerated particles suggest that the two detected reconnection signatures are not from the same reconnection site, indicating that *Cassini* sampled adjacent but independent reconnection channels, a signature consistent with the “drizzle” concept that was suggested by Delamere et al. (2015). In addition, the separation of the two reconnection sites in the azimuthal direction was $\sim 12 R_S$, if considering that they corotate with the magnetosphere (Yao et al. 2017) in the duration over one hour (the time gap of the two reconnection

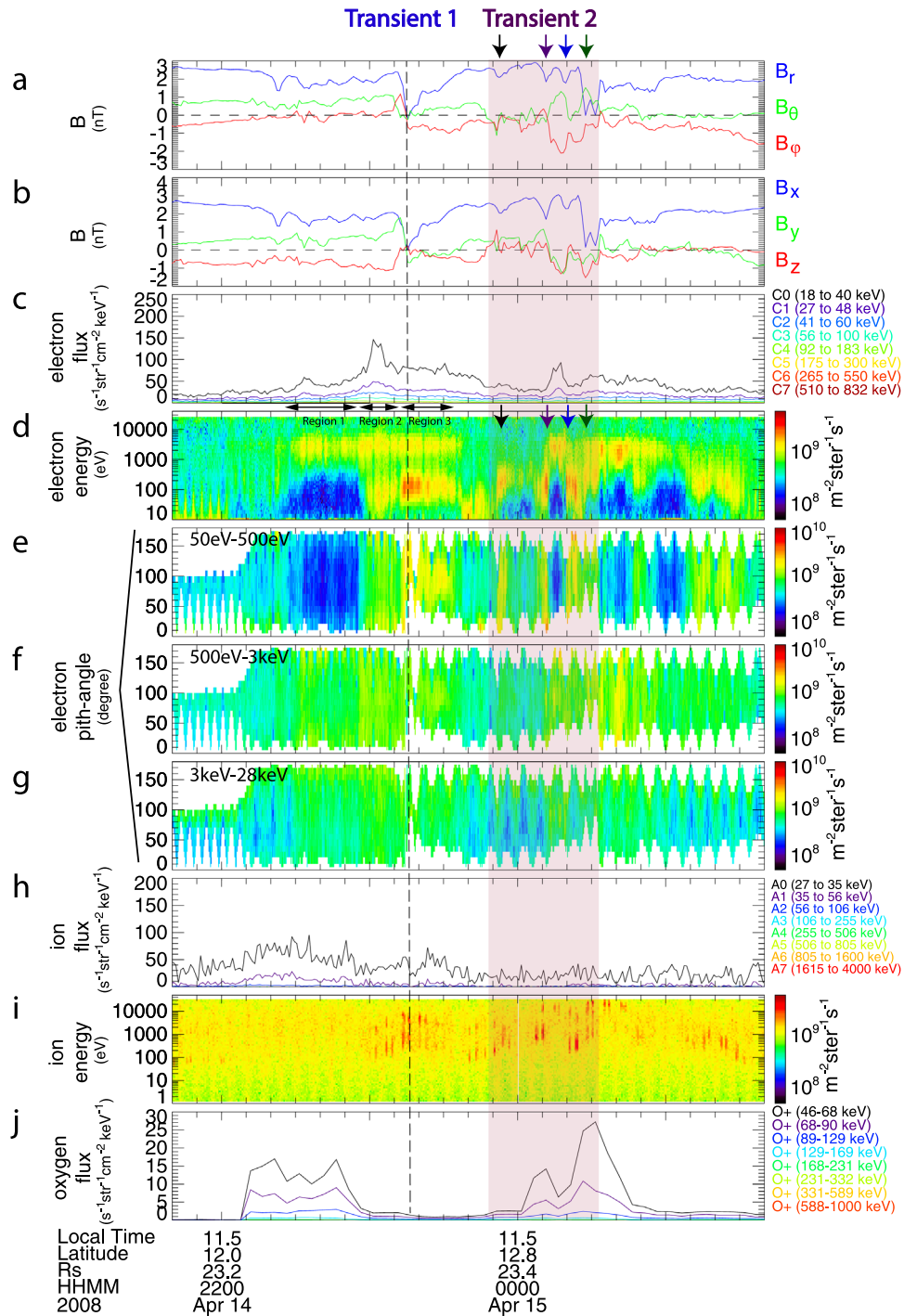


Figure 3. Dayside magnetodisk reconnection event on 2008 April 14th and 15th. The panels are arranged in the same format as Figures 1 and 2. The four colored arrows show the correspondence between the B_r dips and the low-energy electron bands.

events). The large separation between the two reconnection regions may exclude the possibility that they come from different evolution stages of the same event. For the event on 2008 September 15 (Figure 2), there is a long-lasting negative B_θ interval. However, because of the lack of the information on the magnetic structure near the current sheet center, it is hard to determine whether the aforementioned negative B_θ signature is caused by one or more reconnection sites. The B_y signatures are not consistent with the Hall magnetic field signatures outside the negative B_θ regions. This could either be due to the disturbed current sheet, that can result in the X-line coordinates

failing to adequately represent the magnetic geometry near the reconnection region, which is very possible near the current sheet center where the magnetic strength is small; or be due to the interference from the nearby reconnection site if the reconnection process was “drizzle-like.”

The three events show very diverse forms of plasma acceleration, which is naturally expected due to the temporal variations and differences along the *Cassini* trajectories in crossing the complex magnetic reconnection sites in giant planetary magnetospheres. The presence of oxygen ions throughout the magnetosphere introduces an additional layer

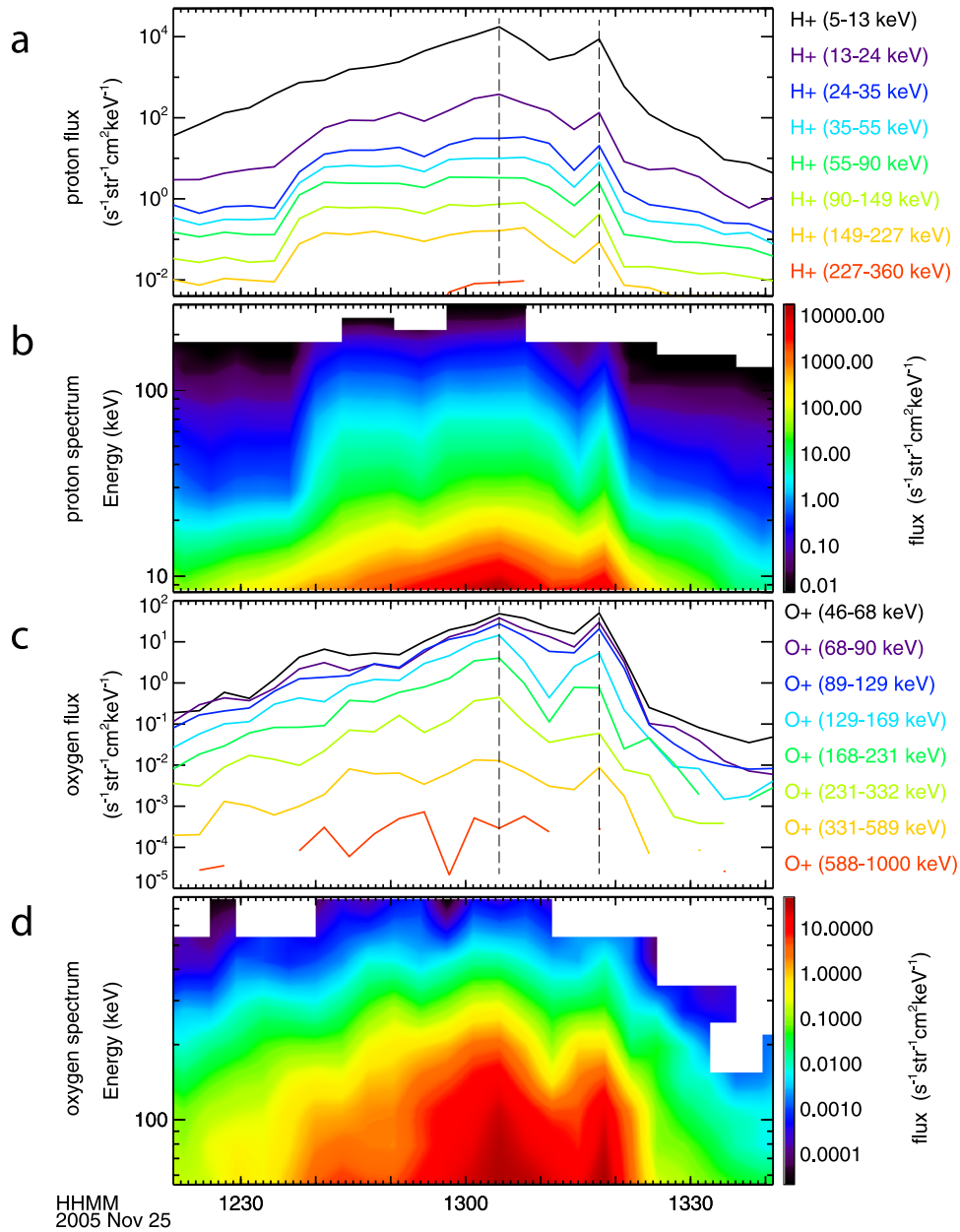


Figure 4. Differential flux and energy spectrogram for the energetic protons (a)–(b) and energetic oxygen (c)–(d) from MIMI-INCA on 2005 November 25, i.e., the first event. There are two major peaks for both protons and oxygen. The fluxes across all energies are enhanced at 13:04 and 13:18 simultaneously.

to the reconnection site, forming an oxygen diffusion region outside the proton diffusion region. This added layer makes the ion diffusion region enlarged and more complex, as particles exhibit different behavior across diffusion regions. For instance, the energetic oxygen ions concentrate in a narrow angular range within the 90×120 degree field of view of MIMI-INCA and peak at the pitch angles neither parallel nor perpendicular, while protons present more isotropic features (not shown, informed from MIMI-INCA). The nongyrotropic and anisotropic feature of the oxygen ions may be due to their non-frozen-in behavior during the acceleration in the diffusion region for their larger gyro-radii (Sergis et al. 2013) comparing to the protons. The efficient perpendicular acceleration on heavy ions has been revealed by Galileo in the Jovian magnetotail reconnection region (Radioti et al. 2007). Combining with the reconnection’s parallel acceleration, it is therefore possible to have accelerated energetic heavy ions at a pitch angle between parallel and

perpendicular as observed in our events. Additionally, the existence of the secondary island in the second event suggests that the reconnection process is not steady, which will increase the diversity in particle behavior. The reason for the double bands in the electron spectrogram in Figure 3(d) and their variation might be very complex as the reconnection can couple different populations (Hesse et al. 2017). We expect this coupling to be more pronounced for “drizzle” reconnection, where multiple plasma populations can be mixed on small spatial scales over a broad magnetospheric region.

In summary, we detailed characteristics of plasma acceleration for three magnetic reconnection events located in the dayside magnetodisk of Saturn. The heavy ions have a strong influence on the evolution of the magnetic reconnection (Liang et al. 2017). Since the content of heavy ions are fundamentally different in giant planets and Earth (Blanc et al. 2015), we would expect a different role of the heavy ions in triggering

reconnection process at Saturn and the Earth's magnetospheres. Unsteady and "drizzle-like" DMR processes at Saturn can energize particles and provide an energy source for exciting auroral emissions connected to Saturn's dayside polar region. Furthermore, if these processes are common and more energetic in Jupiter's magnetosphere, they may offer a crucial means for energizing the heavy ions that precipitate into Jupiter's atmosphere, generating X-ray and UV auroral flares.

This work was supported by the National Science Foundation of China (41704169, 41525016, 41474155, 41274167). Z.Y., D.G., and B.P. acknowledge financial support from the Belgian Federal Science Policy Office (BELSPO) via the PRODEX Programme of ESA. L.C.R. was funded by an STFC Consolidated Grant to Lancaster University (ST/R000816/1). J.H.W. and J.L.B. were supported by NASA JPL contracts 1243218 and 1405851 to the Southwest Research Institute. A.J.C. acknowledges support from the STFC consolidated grants to UCL-MSSL ST/K000977/1 and ST/N000722/1. *Cassini* operations are supported by NASA (managed by the Jet Propulsion Laboratory) and ESA. The data presented in this paper are available from the NASA Planetary Data System <http://pds-ppi.igpp.ucla.edu/>.

ORCID iDs

R. L. Guo  <https://orcid.org/0000-0002-7125-0942>
 Z. H. Yao  <https://orcid.org/0000-0001-6826-2486>
 N. Sergis  <https://orcid.org/0000-0003-4144-8699>
 B. Palmaerts  <https://orcid.org/0000-0003-2762-4334>
 W. R. Dunn  <https://orcid.org/0000-0002-0383-6917>
 L. C. Ray  <https://orcid.org/0000-0003-3727-602X>
 A. J. Coates  <https://orcid.org/0000-0002-6185-3125>
 D. Grodent  <https://orcid.org/0000-0002-9938-4707>
 P. Kollmann  <https://orcid.org/0000-0002-4274-9760>
 J. H. Waite  <https://orcid.org/0000-0002-1978-1025>
 M. K. Dougherty  <https://orcid.org/0000-0002-9658-8085>

References

- Angelopoulos, V., McFadden, J. P., Larson, D., et al. 2008, *Sci*, **321**, 931
 Arridge, C. S., Eastwood, J. P., Jackman, C. M., et al. 2016, *NatPh*, **12**, 268
 Azari, A. R., Liemohn, M. W., Jia, X., et al. 2018, *JGRA*, **123**, 4692
 Badman, S. V., Branduardi-Raymont, G., Galand, M., et al. 2015, *SSRv*, **187**, 99
 Badman, S. V., Masters, A., Hasegawa, H., et al. 2013, *GeoRL*, **40**, 1027
 Bagenal, F., Wilson, R. J., Siler, S., Paterson, W. R., & Kurth, W. S. 2016, *JGRE*, **121**, 871
 Blanc, M., Andrews, D. J., Coates, A. J., et al. 2015, *SSRv*, **192**, 237
 Delamere, P., Otto, A., Ma, X., Bagenal, F., & Wilson, R. 2015, *JGRA*, **120**, 4229
 Dougherty, M. K., Kellock, S., Southwood, D. J., et al. 2004, *SSRv*, **114**, 331
 Drake, J., Swisdak, M., Che, H., & Shay, M. 2006, *Natur*, **443**, 553
 Dungey, J. W. 1961, *PhRvL*, **6**, 47
 Egedal, J., Daughton, W., & Le, A. 2012, *NatPh*, **8**, 321
 Guo, R., Yao, Z., Wei, Y., et al. 2018, *NatAs*, **2**, 640
 Hesse, M., Chen, L., Liu, Y.-H., Bessho, N., & Burch, J. 2017, *PhRvL*, **118**, 145101
 Hones, E. W. 1979, *SSRv*, **23**, 393
 Huddleston, D. E., Russell, C. T., Le, G., & Szabo, A. 1997, *JGR*, **102**, 24289
 Jackman, C., Slavin, J., & Cowley, S. 2011, *JGRA*, **116**, A10212
 Krimigis, S. M., Mitchell, D. G., Hamilton, D. C., et al. 2004, *SSRv*, **114**, 233
 Kronberg, E., Glassmeier, K. H., Woch, J., et al. 2007, *JGRA*, **112**, A05203
 Liang, H., Lapenta, G., Walker, R. J., et al. 2017, *JGRA*, **122**, 618
 Masters, A. 2017, *JGRA*, **122**, 11154
 McAndrews, H., Owen, C., Thomsen, M., et al. 2008, *JGRA*, **113**, A04210
 Mitchell, D. G., Krimigis, S. M., Paranicas, C., et al. 2009, *P&SS*, **57**, 1732
 Palmaerts, B., Radioti, A., Roussos, E., et al. 2016a, *JGRA*, **121**, 11952
 Palmaerts, B., Roussos, E., Krupp, N., et al. 2016b, *Icar*, **271**, 1
 Paschmann, G., Sonnerup, B. Ö., Papamastorakis, I., et al. 1979, *Natur*, **282**, 243
 Radioti, A., Woch, J., Kronberg, E. A., et al. 2007, *JGRA*, **112**, A06221
 Roussos, E., Krupp, N., Mitchell, D. G., et al. 2016, *Icar*, **263**, 101
 Sergis, N., Arridge, C. S., Krimigis, S. M., et al. 2011, *JGRA*, **116**, A04203
 Sergis, N., Jackman, C. M., Masters, A., et al. 2013, *JGRA*, **118**, 1620
 Slavin, J. A., Acuña, M. H., Anderson, B. J., et al. 2009, *Sci*, **324**, 606
 Vasyliunas, V. 1983, in *Physics of the Jovian Magnetosphere*, Vol. 1, ed. A. J. Dessler (Cambridge: Cambridge Univ. Press), 395
 Wang, S., Chen, L. J., Bessho, N., et al. 2016, *JGRA*, **121**, 2104
 Yao, Z., Coates, A., Ray, L., et al. 2017, *ApJL*, **846**, L25
 Yates, J. N., Southwood, D. J., Dougherty, M. K., et al. 2016, *GeoRL*, **43**, 11102
 Young, D., Berthelier, J., Blanc, M., et al. 2004, *SSRv*, **114**, 1
 Zweibel, E. G., & Yamada, M. 2009, *ARA&A*, **47**, 291